S1 Meteorological conditions

The seasonal variation for the temperature (T), wind speed (WS), and relative humidity (RH) in the HMA during 2009 – 2018 are presented in Fig. S1a-c, and the time series for these parameters are presented in Fig. S1d-f. The variation of WS is studied in more detailed in Fig. S2, which presents the diurnal variation of the WS separately for the cold (November – March) and the warm seasons (May – September). All the meteorological data presented in the supplementary is measured at the weather observation site, which is presented in Sect. 2.1.4.

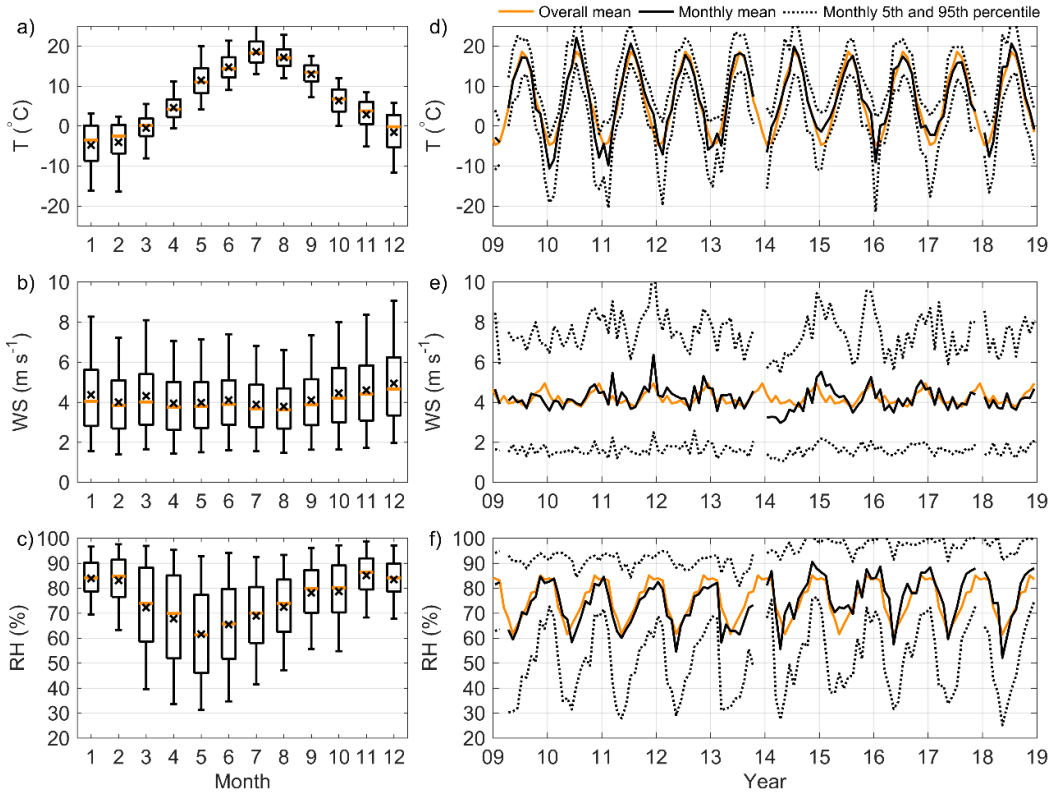

Figure S1: The monthly statistics of different meteorological parameters on the left panel: a) T, b) WS, and c) RH. The orange line in the middle of each box represents the median, the edges of the boxes represent the 25th and 75th percentiles, and the whiskers represent the 5th and 95th percentiles. The black cross is the arithmetic mean. On the right panel are the time series for d) T, e) WS, and f) RH. The statistical values were determined from 1 h averaged data.

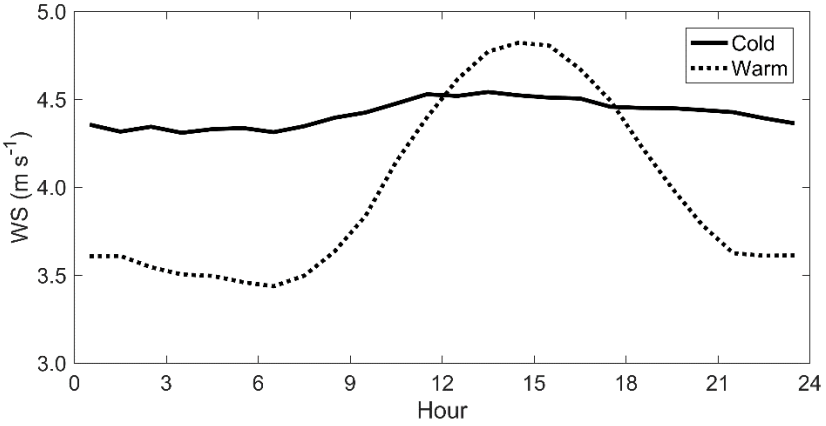

Figure S2: The mean diurnal variation of WS for the cold (November – March) and warm (May – September) seasons. The diurnal variation was calculated from 1 h mean values.

S2 Detailed description of the measurement sites

This sections represents more detailed descriptions from each site. Figure S3 represents the aerial photos from each traffic site (TR) and it also shows the names of the closest streets or roads. Figure S4 represents the aerial photos from each detached housing sites (DH). Figure S5 represent the aerial photos from both urban background (UB) and regional background (RB) sites. The size scale is about same in all the subfigures.

The coordinates for each station are given in Table S1, which also lists all the used instruments for measuring equivalent black carbon concentration (eBC), the mass of particles smaller than 2.5 µm ($PM_{2.5}$), and NO_x.

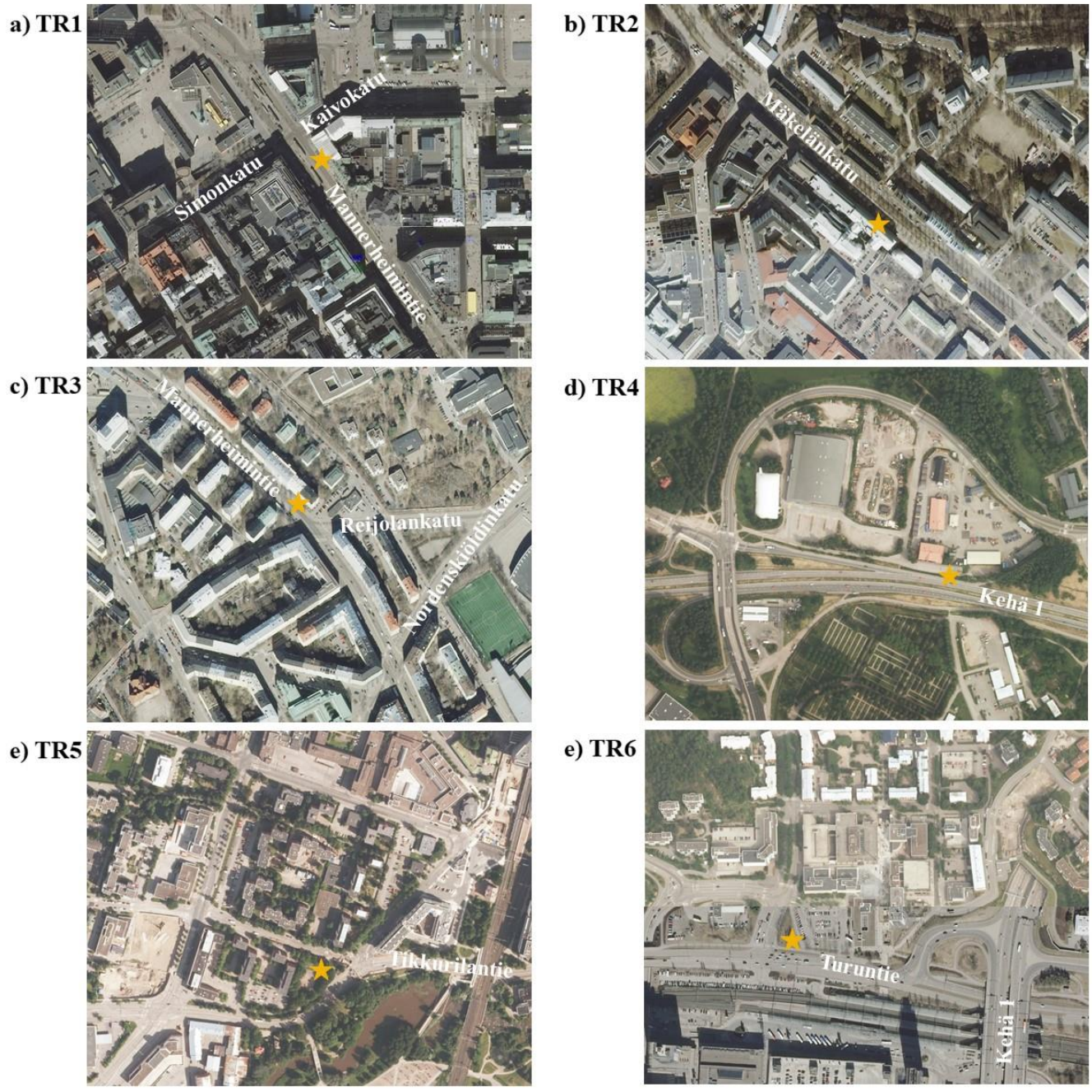

Figure S3: The aerial pictures of the traffic sites. The location of the station is marked with a star. The size range on the East – West direction is about 600 m and on the North – South direction around 460 m. The pictures are modified (street names and the location of the station were added) from the orthophotos provided by the National Land Survey of Finland (02/2020).

Figure S4: The aerial pictures of the stations located in the detached house areas. The location of the station is marked with a star. The size ranges are the same as in Fig. S3. The pictures are modified (location of the station was added) from the orthophotos provided by the National Land Survey of Finland (02/2020).

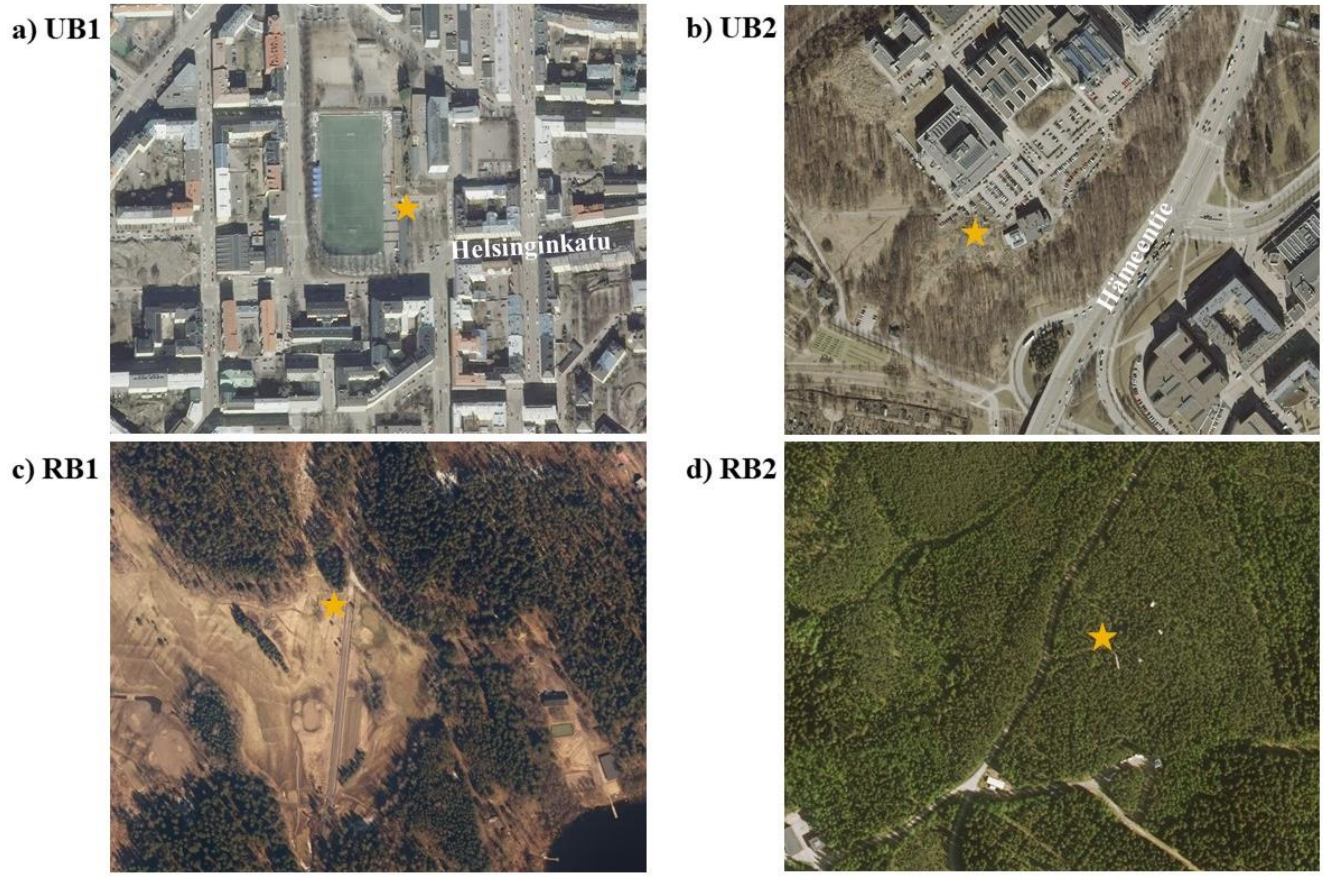

Figure S5: The aerial pictures of the background stations. The location of the station is marked with a star. The size ranges are the same as in Fig. S3. The pictures are modified (location of the station was added) from the orthophotos provided by the National Land Survey of Finland (02/2020).

Table S1: Detailed information about the eBC measurements at different stations. FH 62 I-R determines the aerosol mass concentration by measuring the attenuation of β-radiation, TEOM uses an oscillating microbalance method and Grimm measures the mass by optical means.

Station	Coordinates	eBC instrument	$PM_{2.5}$ instrument	NO_x instrument	Operator
TR1	60°10'10.6''N 24°56'21.5''E	MAAP	FH 62 I-R	Horiba APNA 370	HSY
TR2	60°11'47.1''N 24°57'07.4''E	MAAP	TEOM 1405, TEOM 1400 AB	Horiba APNA 370	HSY
TR3	60°11'24.1''N 24°54'57.7''E	MAAP	TEOM 1400 AB	Horiba APNA 370	HSY
TR4	60°14'30.7''N 25°01'32.5''E	MAAP	TEOM 1400 AB	Horiba APNA 370	HSY
TR5	60°17'23.8''N 25°02'22.4''E	MAAP	TEOM 1400 AB, TEOM 1405	Horiba APNA 370	HSY
TR6	60°13'13.0''N 24°48'40.9''E	MAAP	FH 62 I-R	Horiba APNA 370	HSY
DH1	60°13'26.5''N 25°06'09.4''E	MAAP	Grimm 180	Horiba APNA 370	HSY
DH2	60°18'43.4''N 25°00'39.9''E	MAAP	FH 62 I-R	Horiba APNA 360	HSY
DH3	60°14'21.9''N 24°48'49.4''E	MAAP	FH 62 I-R	Horiba APNA 360	HSY
DH4	60°19'53.2''N 25°04'33.2''E	MAAP and AE33	FH 62 I-R	Horiba APNA 360	HSY
DH5	60°17'30.2''N 25°06'46.3''E	AE33	FH 62 I-R	Horiba APNA 370	HSY
UB1	60°11'14.5''N 24°57'02.3''E	MAAP	TEOM 1405, TEOM 1400 AB	Horiba APNA 370, Thermo 42i	HSY
UB2	60°12'10.4''N 24°57'40.4''E	MAAP	TEOM 1405D	API 200AU, Horiba APNA 360	FMI, UHEL
RB1	60°18'51.7''N 24°41'04.6''E	MAAP	FH 62 I-R	Horiba APNA 370	HSY

RB2	61°50’47.5’’N 24°17’40.1’’E	MAAP and AE31	Cascade-impactor and manual weightings	TEI 42CTL and 42iTL with photolytic converter	UHEL

S3 AE31 and MAAP comparison at RB2

The comparison between the Aethalometer model AE31 and Multi-Angle Absorption Photometer (MAAP) is shown in Fig. S6. The comparison includes data measured during July 2013 – December 2018, when MAAP was measuring in parallel with AE31. The BC data measured with the AE31 at wavelength 880 nm was corrected by using the correction algorithm described by Virkkula et al. (2007) and the data was compared against the concentration measured by MAAP at wavelength 637 nm.

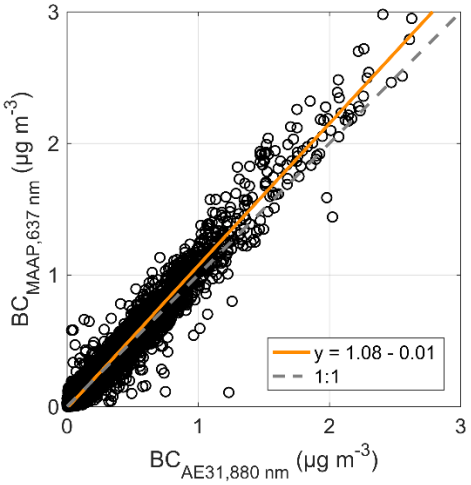

Figure S6: Relation between eBC measured by MAAP and AE31 at RB2. The orange line is the linear fit and the grey dashed line is the 1:1 line.

S4 Correlation between eBC and other air pollutants

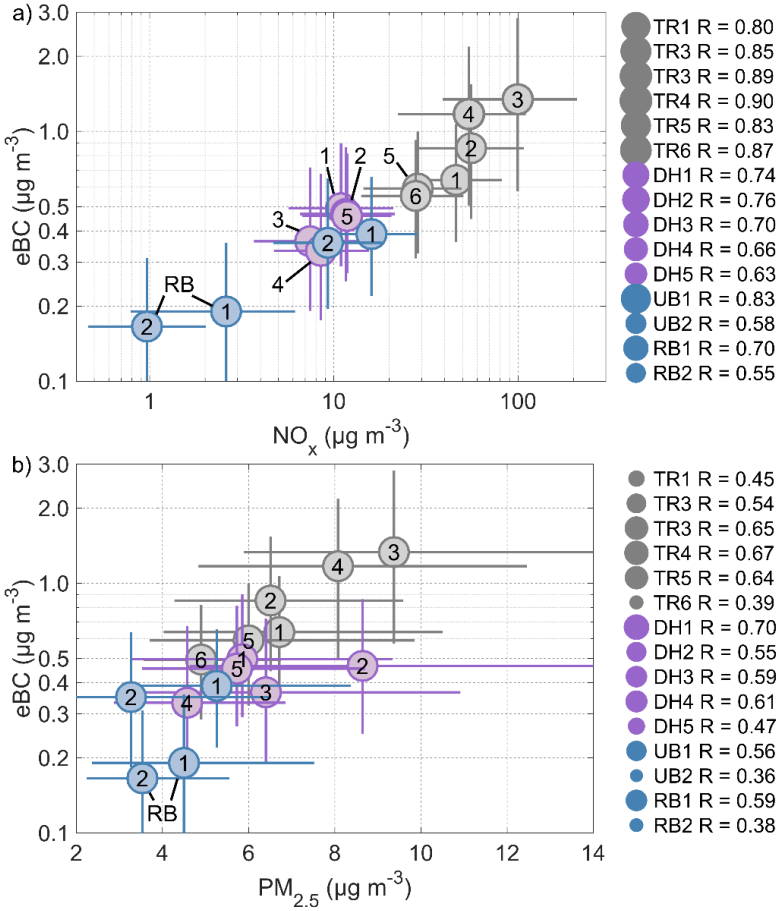

Figure S7: The relation between a) eBC and NO_x concentration, and b) eBC and $PM_{2.5}$ concentration. The circles mark the median eBC, NO_x and $PM_{2.5}$ values and the whiskers are the 25th and 75th percentiles of all the available data for each station. The grey markers represent the traffic stations, purple represent the detached housing stations, and the blue markers represent the background sites. The correlation between the variables at each station are presented on the right side, where the marker size represents the correlation coefficient.

S5 Trends at TR3

The eBC concentration at TR3 showed clear decrease between the years 2010 and 2015. However, since there were only two years of measurements, we could not apply the seasonal Kendall test to see if there was a statistically significant decreasing trend. Therefore, we ran a Mann-Whitney U-test for the TR3 air pollution data to see if difference in the median values between these two years (1.83 and 1.00 μg m^{-3} for 2010 and 2015, respectively) were statistically significant. The test showed a statistically significant difference (p-value << 0.01) between the median values of the annual eBC concentration. According

to the annual medians, the median decreased 0.17 µg m^{-3} yr^{-1} (-12 % yr^{-1}). With a similar analysis, we got decrease of 8 µg m^{-3} yr^{-1} (-8 % yr^{-1}) and -0.6 µg m^{-3} yr^{-1} (-7 % yr^{-1}) for the NO_x and $PM_{2.5}$ data.

One reason for the decrease in the concentrations of different air pollutants is probably the decrease in traffic counts next to the site. In 2010 the traffic count on the street next to the TR3 was estimated to be 44 400 vehicles per weekday and in 2015 the estimated traffic count had decreased to 33 500 vehicles per weekday.

In addition to the traffic count, also different meteorological conditions might explain the notable decrease in the air pollutant concentrations. The difference in the meteorological parameters (T and WS) in 2010 and 2015 are compared in Fig. S8. The figure shows that in 2010, when the eBC concentration was notably higher, the T was actually much lower during the winter in 2010 than in 2015. Also, the WS was lower during the winter in 2010 compared to 2015. During summer, the T is a bit higher in 2010 than in 2015. Teinilä et al., (2019) showed that the most important meteorological parameters explaining the eBC concentration are the T and WS, so that the highest pollutant concentrations are measured during calm winds when the temperature is either cold or hot. Therefore, the annual variation of T and WS most probably explain at least part of the high concentrations measured at TR3 in 2010. This example shows that the meteorological parameters might have a big effect on the year-to-year-variation of the air pollutant concentrations.

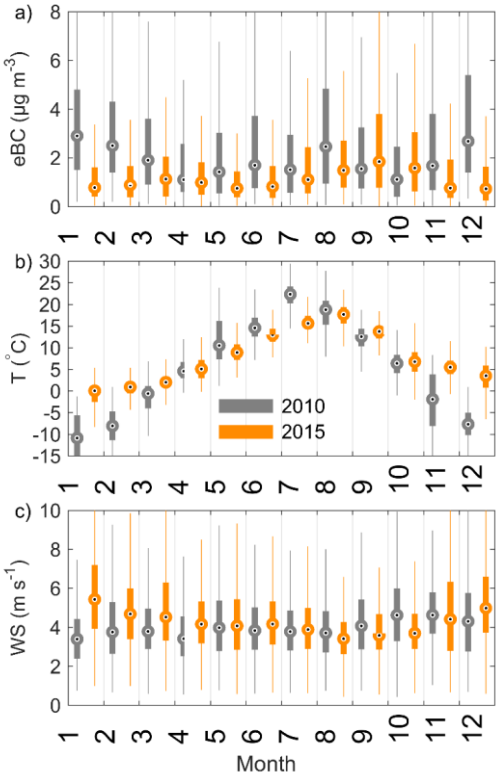

Figure S8: The statistics of the a) eBC concentration at TR3, b) temperature, and c) wind speed in 2010 and 2015.

S6 Traffic counts in the HMA

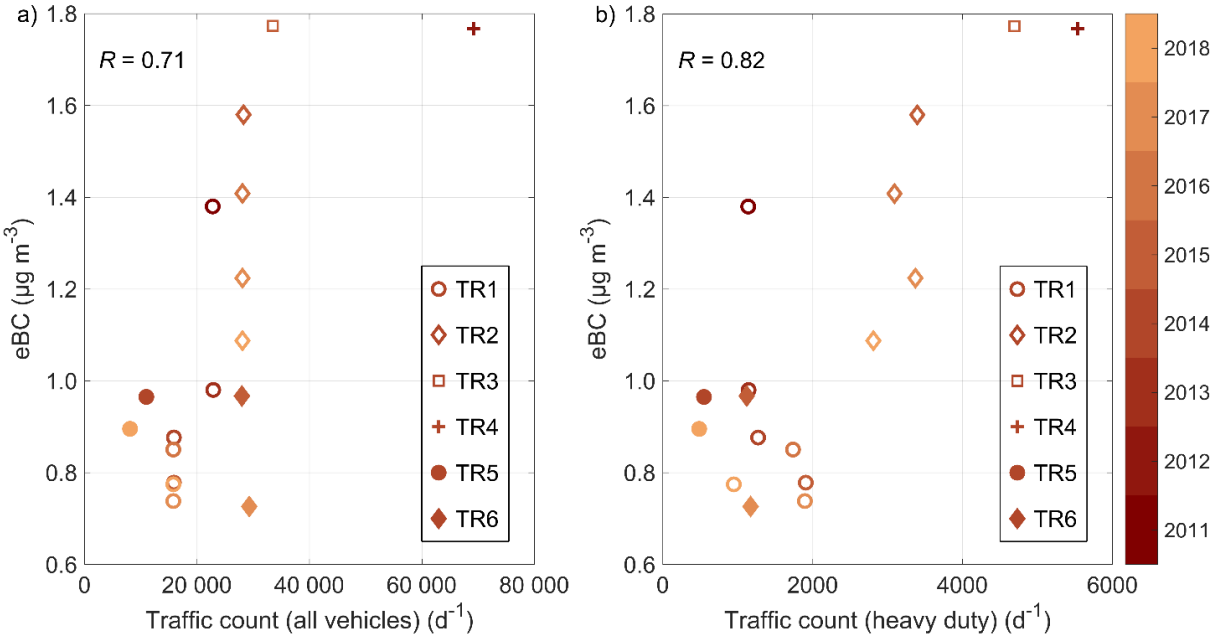

Figure S9: The relation between a) eBC concentration and total traffic count, and b) eBC concentration and the traffic count of heavy-duty vehicles only for each station and year separately. The eBC values are annual means, which were determined for weekdays only. The traffic counts are estimates for the closest street on a weekday. The estimates were provided in the yearly traffic reports by the city of Helsinki. The data from TR3 in 2010 and TR5 in 2016 were omitted, since there was no estimation for the heavy-duty traffic count.

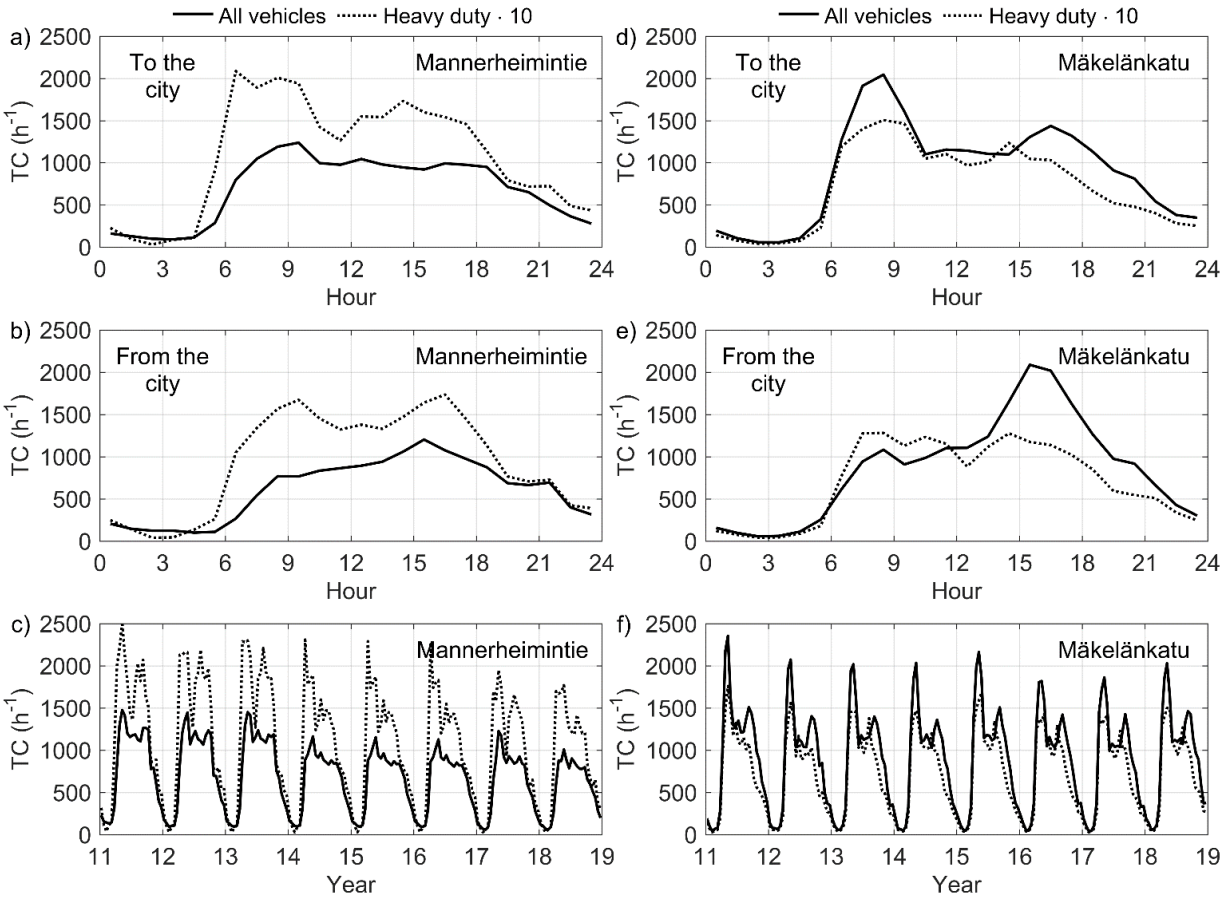

Figure S10: Traffic counts (TC) at a) – c) Mannerheimintie and d) – e) Mäkelänkatu streets. Here, the measurement point at Mannerheimintie located about 2 km North of TR3 and the measurement point at Mäkelänkatu located about 400 m North-West of TR2, so the TC does not necessarily represent the traffic at TR3 and TR2. Note that the TC of heavy-duty is multiplied by 10 to make the comparison easier. Mean traffic count for each hour in the traffic lanes that lead towards the city centre are presented in subfigures a) and d), and subfigures b) and e) represent the diurnal variation in the traffic lanes that lead away from the city centre. Subfigures c) and f) present the diurnal traffic count for each year. The traffic count data was provided by the Helsinki Region Infoshare (06/2019).

S5 Temporal variation

In this section, we provide supplementary material and more detailed information about the variation of eBC. Figure S11 is similar to Fig. 2, but here the spatial variation is represented separately for the cold and the warm seasons. The seasonal variation and the diurnal variation for each station separately are represented in Figs. S12 and S13, respectively.

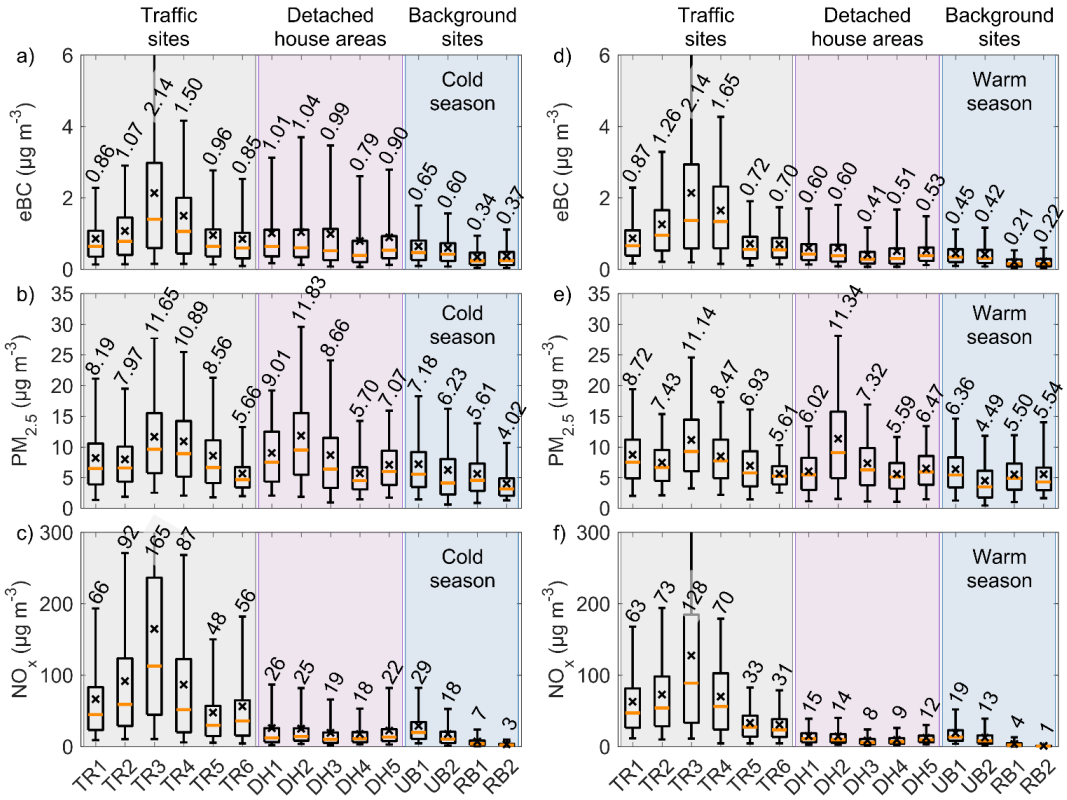

Figure S11: The statistics of the eBC, $PM_{2.5}$, and NO_x concentrations at each station separated for the cold (November – March; left column) and warm (May – September; right column) season. The boxplots have been calculated from 1 h mean values. The explanation for the boxes are the same as in Fig. S1. The mean values are reported above each box. The background color represents the station type: gray for TR sites, purple for the DH sites, and blue for the background (UB and RB) sites.

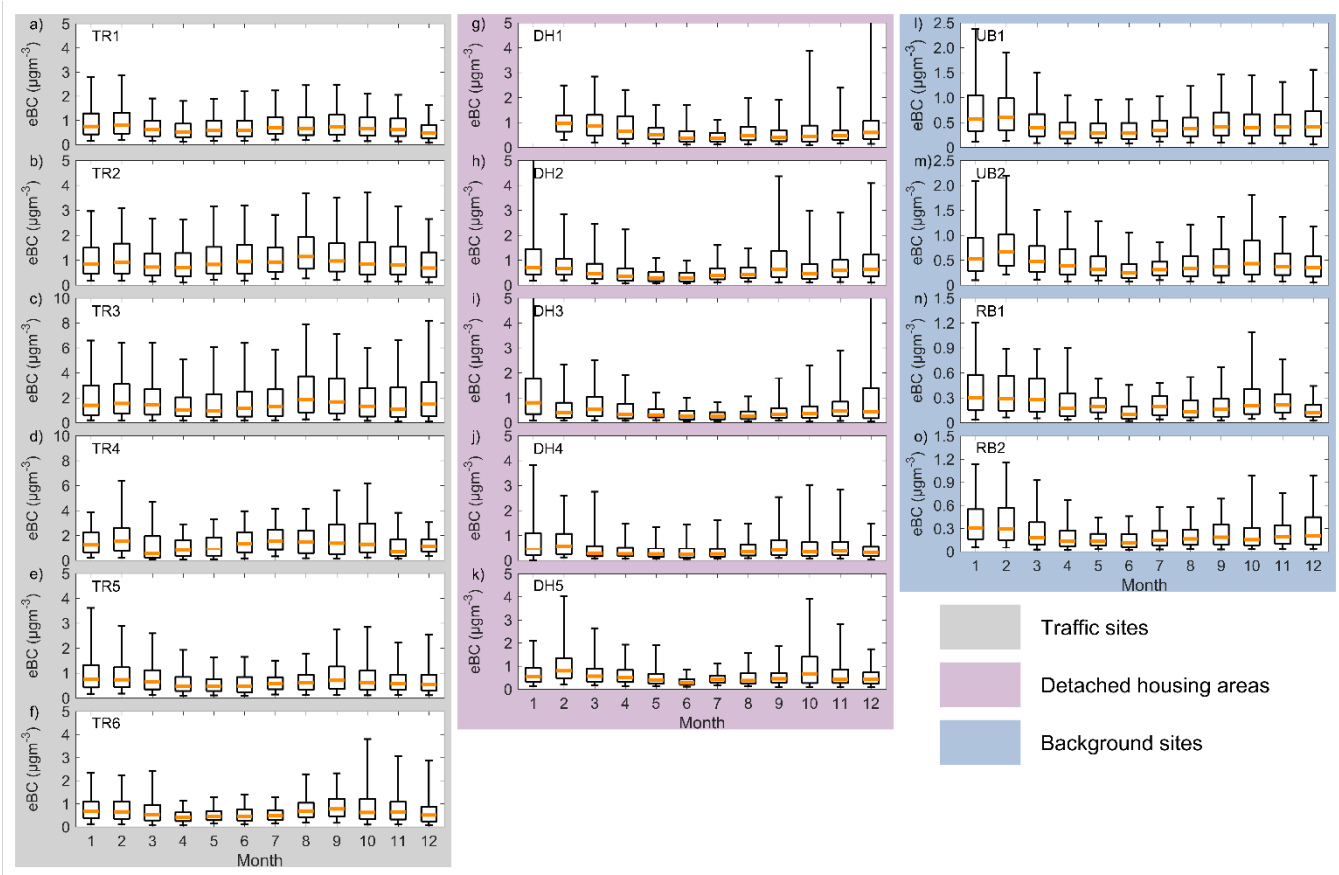

Figure S12: Seasonal variation for each station separately. The explanation for the boxes is the same as in Fig. S1.

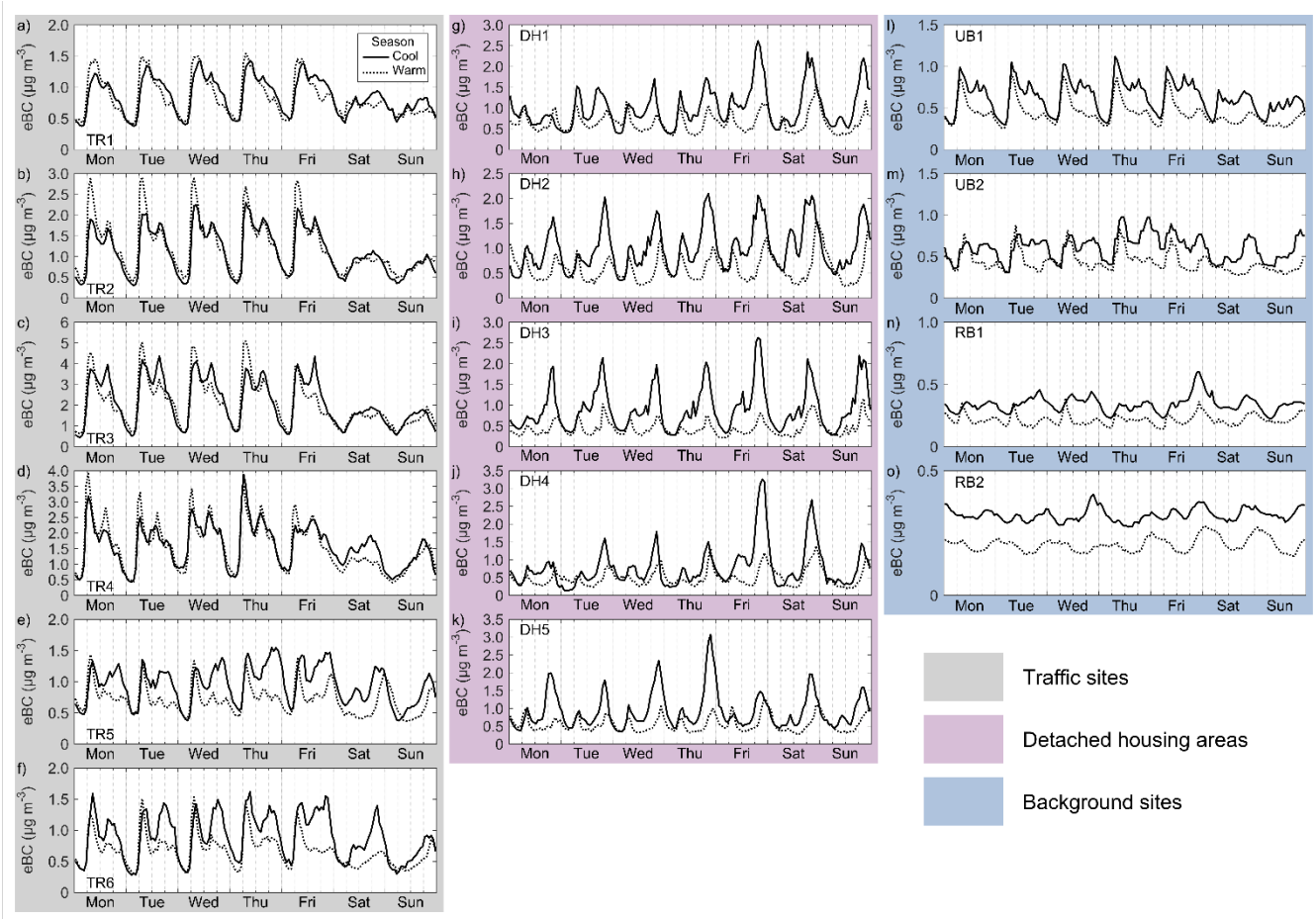

Figure S13: Similar to Fig. 6, but here the diurnal variation is represented at each site.

Figure S15 represents the diurnal variation of the eBC/$PM_{2.5}$ ratio. In general the eBC/$PM_{2.5}$ ratio seemed to follow the variation of eBC (i.e. the eBC varies relatively more than $PM_{2.5}$). As the lowest eBC concentration (Fig. 6), the lowest eBC/$PM_{2.5}$ ratio at the TR, DH, and UB sites occurred around 3 a.m. and it is about 5 %, which is close to the median eBC/$PM_{2.5}$ fraction at the RB sites (about 4.3 %). At TR1-4, there seemed to be no large seasonal variation in the eBC/$PM_{2.5}$ ratio. At TR5-6, the eBC/$PM_{2.5}$ ratio seemed to be slightly higher during the cool season, whereas at the DH, UB, and RB sites the eBC/$PM_{2.5}$ fraction was clearly higher during the cool season.

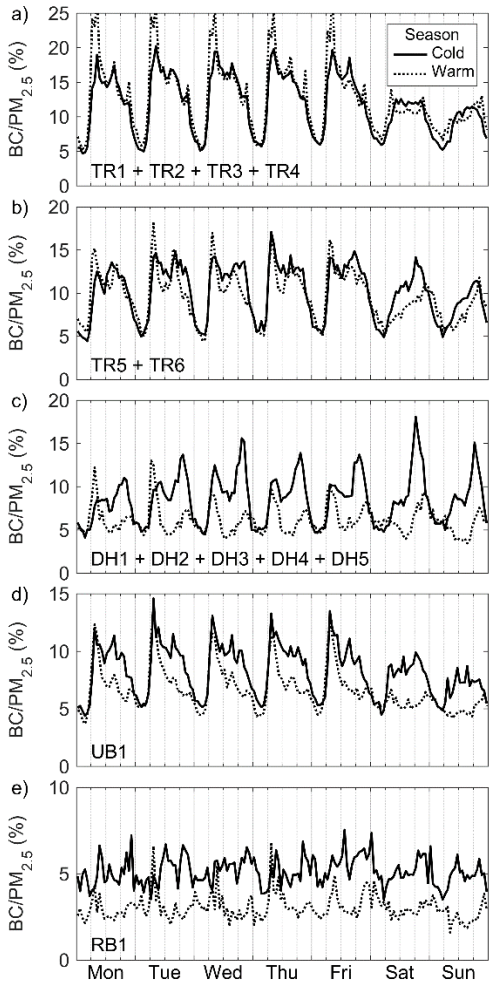

Figure S14: Median diurnal variation of the BC/$PM_{2.5}$ fraction. Here the fraction is presented as median, since the data is noisy and the variation is not well visible with the mean values.